[2] Jones, D. J., "Tables of Inviscid Supersonic Flow About Circular Cones at Incidence, $\gamma = 1.4$," AGARDograph No. 137, Nov. 1969.
[3] Sears, W. R., *"General Theory of High Speed Aerodynamics,* Vol. 6, Oxford University Press, 1955, pp. 238–239.
[4] Cheng, H. K., "Hypersonic Shock Layer Theory of a Yawed Cone and Other Three Dimensional Bodies," *Journal of Fluid Mechanics,* Vol. 12, No. 2, 1962, p. 169.
[5] Lees, L., "Note on the Hypersonic Similarity Law for an Unyawed Cone," *Journal of the Aeronautical Sciences,* Vol. 18, 1951, pp. 700–702.
[6] Rasmussen, M. L., "On Hypersonic Flow Past an Unyawed Cone," *AIAA Journal,* Vol. 5, No. 8, Aug. 1967, pp. 1495–1497.
[7] Chernyi, G. G., *Introduction to Hypersonic Flow,* Academic Press, New York, 1961, pp. 113–120.

Analysis of Jimsphere Wind Profiles Viewed in the Flight Time Domain of a Saturn Vehicle

S. I. ADELFANG*
Lockheed-California Company, Burbank, Calif.

NINE hundred Jimsphere wind profiles obtained over Cape Kennedy, Fla., between November 1964 and May 1967 were used for an analysis of horizontal wind speeds viewed by a Saturn vehicle in an AS-504 trajectory. Each profile was evaluated at $\frac{1}{6}$-sec intervals of AS-504 vehicle flight time and high-pass-filtered to remove low-frequency fluctuations that would not involve significant control and structural responses in the vehicle. This paper describes the distribution of gusts, gust variance, and spectrum densities observed in these profiles.

Gust Profile Definition

Vehicle response characteristics are usually defined in terms of temporal frequency f (cps) rather than spatial frequency K (cpm). As a vehicle ascends with vertical velocity $v(t)$ through the atmosphere, wind fluctuations at spatial frequency K are seen by the vehicle at frequency f given by

$$f = Kv(t) \tag{1}$$

Thus, for example, the fluctuations in the wind profile at $K = 2.74.10^{-3}$ (cpm) as seen by a Saturn vehicle increase from $f = 0.534$ cps at 4 km ($v = 195$m/sec) to $f = 1.00$ cps at 12 km ($v = 365$m/sec). Since the first bending mode frequency of a Saturn 5 vehicle is approximately 1 cps, the fluctuations at $K = 2.74.10^{-3}$ cpm are more important at 12 km than at 4 km. Innumerable spatial frequencies exist for a particular critical value of temporal vehicle response frequency; therefore, it is necessary to transform the spatial fluctuations of wind profiles to temporal fluctuations as seen by the vehicle.

The general procedure suggested in Ref. 1 for deriving gust profiles is used for this study. Jimsphere wind profiles are transformed to vehicle time coordinates by evaluating them at altitudes Z (km) corresponding to the time, t (sec), from launch at intervals of time Δt (sec), according to the least-squares quadratic fit to the Saturn AS-504 trajectory given by Jacobs[2]:

$$Z = 2.98416 - 0.14889t + 0.00330t^2 \tag{2}$$

Z calculated from Eq. (2) deviates less than 1.7% from the AS-504 trajectory for the time interval from 50 to 95 sec ($Z = 3.855$ to 18.530 km). The time interval Δt was chosen small enough to include all Jimsphere data up to 17.2 km. Assuming that a Jimsphere profile contains independent estimates of wind over 75 m altitude intervals, the time interval Δt (sec) between independent wind estimates as seen by a vehicle is $75/v(t)$; at 17.2 km, for Saturn AS-504, $v(t) = 450$ m/sec, hence $\Delta t = \frac{1}{6}$ sec.

The transformed wind profile is an approximation of the profile "seen" by the vehicle; the accuracy of the approximation for space vehicle studies is not yet known and may only be determined when the statistics of vehicle responses derived from simulated flights through Jimsphere wind profiles are compared to the same statistics derived from wind profile data obtained from sensors which traverse the atmosphere in space-time coordinates that are similar to those of space vehicles.

The fluctuations of interest, which will be referred to as gusts, are characterized by their influence on space vehicle control and structural excitation frequency modes. For a Saturn vehicle significant response to wind fluctuations occur at the control frequency (~0.2 cps) and at the first and second bending mode frequencies (~1.2 cps). Wind profiles which have fluctuations at frequencies ≥0.2 cps are defined as gust profiles. Gust profiles were calculated by application of a 33 weight digital high-pass filter which has a transfer function of the form

$$H(f) = 1 - \exp[-39.2f/f_s]^2 \tag{3}$$

Table 1 Symmetrical 33 weight digital high-pass filter with transfer function given by Eq. (4); $\Delta t = \frac{1}{6}$ sec

Time	Numerical weights
t	0.951844
$-\Delta t + \Delta t$	−0.047848
$-2\Delta t + 2\Delta t$	−0.046936
$-3\Delta t$, etc.	−0.045453
...	−0.043457
...	−0.041013
...	−0.038222
...	−0.035162
...	−0.031935
...	−0.028634
...	−0.025346
...	−0.022151
...	−0.019110
...	−0.016288
...	−0.013689
...	−0.011364
$-16\Delta t$, $+16\Delta t$	−0.009314

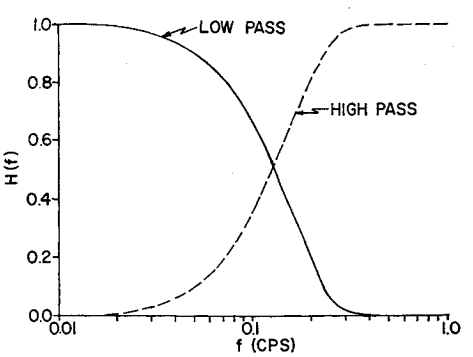

Fig. 1 Transfer functions of Alfriend exponential low-pass and high-pass filters for a sampling frequency of 6 sec^{-1}.

Received May 4, 1970; revision received June 19, 1970. The author expresses his appreciation to the Aerospace Environment Division, Aero-Astrodynamics Laboratory, NASA, Huntsville, Ala. for their support of this research under Contract NAS 8-30165.

* Research Scientist.

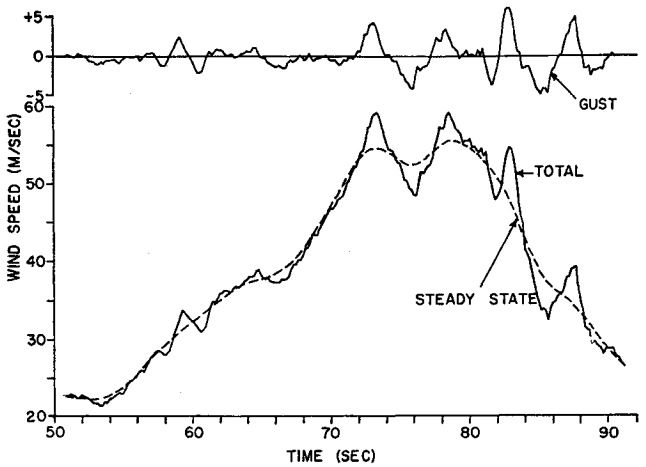

Fig. 2 Jimsphere wind profile 477, transformed to Saturn AS-504 time coordinates (solid line), steady-state or low-pass-filtered (dashed line) and gust or high-pass-filtered as labeled.

where f = frequency (cps). Since f_s, the data sampling frequency, is 6 sec^{-1}, Eq. (3) reduces to

$$H(f) = 1 - \exp(-6.53f)^2 \quad (4)$$

The 33-point weighting function (listed in Table 1) for the high-pass filter was calculated by subtracting the weighting function of the low-pass filter described by Alfriend[3] from the weighting function of an all-pass filter (an all-pass filter has weights equal to zero except for the middle weight, which is unity). The transfer function of the Alfriend low-pass filter for f_s = 6 sec^{-1} is

$$H(f) = \exp(-6.53f)^2 \quad (5)$$

The transfer functions of the high-pass and low-pass filters described by Eqs. (4) and (5) are illustrated in Fig. 1. The

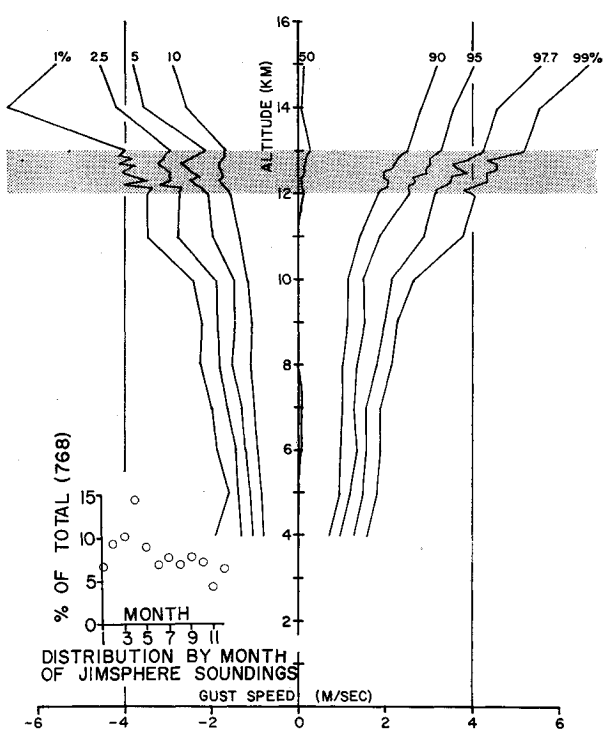

Fig. 3 Gust distribution computed from 794 Cape Kennedy Jimsphere profiles; the distribution by month is illustrated in the lower left.

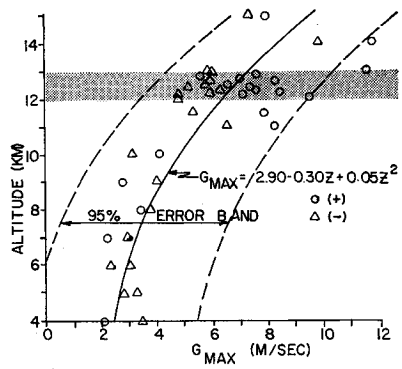

Fig. 4 Maximum observed absolute gust speed vs altitude in 794 profiles.

relation between the low-pass and high-pass-filtered profile and the total profile is illustrated in Fig. 2 for Cape Kennedy Jimsphere profile 477; the total profile transformed to Saturn AS-504 time coordinates is represented by the solid line; the low-frequency or low-pass-filtered profile, which has been termed the steady-state wind profile with respect to the Saturn AS-504 in Ref. 1, is illustrated by the dashed line; the gust or high-pass-filtered profile, which is the total profile minus the low-pass-filtered profile, is illustrated across the top of the figure.

Statistical Analysis

The Jimsphere gust profiles were analyzed to determine the distribution of gusts as a function of altitude, gust variance as a function of Saturn AS-504 flight time interval, and spectrum densities of gusts. The percentile distributions of gusts as functions of altitude are illustrated in Fig. 3, based on the 794 profiles that had gust data between 4 and 15 km. The percentiles are plotted at altitude intervals of 1 km between 4 and 15 km, and 100 m between 12 and 13 km. The gust magnitudes at the extreme percentiles ($\geq$90%, $\leq$10%) generally increase with altitude; the variability of gust magnitudes for small-scale variations of altitude is illustrated by the data given at 100 m intervals between 12 and 13 km. The maximum observed absolute gust speed (G_{max}, m/sec) as a function of altitude (km) is illustrated in Fig. 4; the solid line in the figure is the least-squares quadratic function fitted

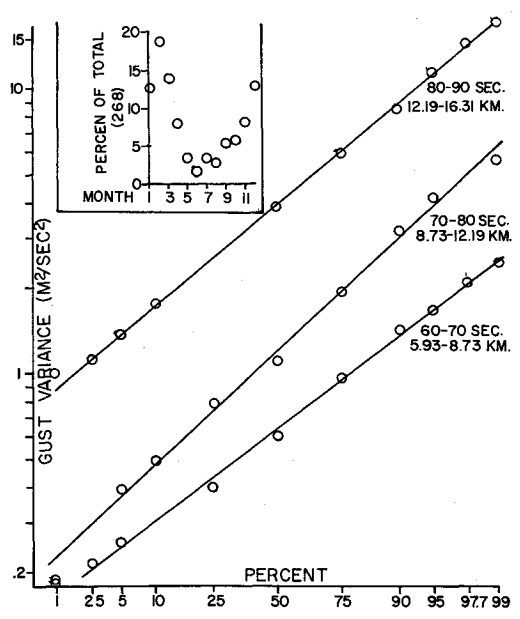

Fig. 5 Cumulative distribution of gust variance computed for 268 Jimsphere profiles for three 10-sec intervals of Saturn AS-504 flight time; at upper left is distribution by month.

Table 2 Minimum, maximum, and cumulative percent frequency distribution of power spectrum densities of 900 Jimsphere gust profiles

Frequency, cps	Min.	Cumulative frequency, % 1.0	2.3	5.0	10	25	50	75	90	95	97	99	Max.
						(m/sec)²/(cycle/ft)							
0.3	0.3728	0.5535	0.6612	0.7731	0.9057	1.3092	1.9327	2.6919	3.5582	4.4052	5.2680	5.7102	7.9160
0.6	0.1365	0.1583	0.1975	0.2317	0.2780	0.3672	0.5123	0.6993	0.8798	1.0055	1.1828	1.3697	1.7266
0.9	0.0490	0.0625	0.0692	0.0813	0.0941	0.1199	0.1613	0.2164	0.2650	0.2983	0.3358	0.3650	0.6652
1.2	0.0202	0.0243	0.0303	0.0351	0.0402	0.0526	0.0690	0.0896	0.1172	0.1345	0.1537	0.1760	0.3916
1.5	0.0107	0.0150	0.0166	0.0185	0.0212	0.0285	0.0374	0.0510	0.0681	0.0868	0.1022	0.1374	1.1941
1.8	0.0063	0.0079	0.0097	0.0108	0.0127	0.0175	0.0237	0.0332	0.0497	0.0658	0.0837	0.1066	0.1583
2.1	0.0037	0.0052	0.0059	0.0070	0.0085	0.0114	0.0161	0.0241	0.0381	0.0554	0.0718	0.1024	0.1453
2.4	0.0021	0.0037	0.0043	0.0052	0.0061	0.0082	0.0120	0.0185	0.0309	0.0453	0.0676	0.0959	0.1621
2.7	0.0014	0.0029	0.0035	0.0040	0.0048	0.0066	0.0098	0.0157	0.0269	0.0412	0.0619	0.0896	0.1703
3.0	0.0013	0.0023	0.0026	0.0032	0.0041	0.0060	0.0093	0.0144	0.0267	0.0384	0.0578	0.0904	0.1555

to the data

$$G_{max} = 2.90 - 0.30Z + 0.05Z^2 \quad (6)$$

Figure 5 illustrates the cumulative percentile distribution of gust variance (m^2/sec^2) for three Saturn vehicle flight time intervals of 60–70, 70–80, and 80–90 sec; these time intervals correspond to Saturn altitude intervals of 5.93 to 8.73, 9.73 to 12.19, and 12.19 to 16.31 km, respectively. The cumulative distribution is approximately log-normal as indicated by the straight lines fitted to the plotted points.

Power spectrum densities (PSD's) of 900 Jimsphere gust profiles defined in the time domain of a Saturn vehicle were computed according to the method described by Blackman and Tukey.[4] The 900 profiles were selected on the basis of completeness between 4 and 14 km. A Saturn vehicle in an AS-504 trajectory requires 36 sec to traverse the 4- to 14-km altitude interval; thus a gust profile evaluated at $\frac{1}{6}$-sec intervals according to Eq. (1) would contain 216 data points. PSD's, computed using 10 lags, are given at intervals of 0.3 cps from 0.3 to 3.0 cps. The cumulative percentile distribution of the PSD's [(m/sec)²/(cycle/sec)] at each frequency is given in Table 2.

In Fig. 6 the PSD's at the median and the 95 and 99 percentiles are compared with recent updated MSFC design criteria spectra[5] derived in the altitude domain from a similar set of Cape Kennedy Jimsphere wind profiles. The direct comparison is valid only if the MSFC PSD's $\Phi(K)$ [(m/sec)²/(cycle/4000 m)], originally expressed as a function of spatial

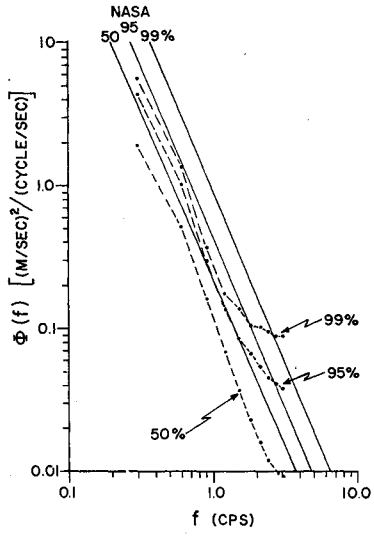

Fig. 6 Medium and 96 and 99% upper bounds of PSD of 900 Jimsphere wind speed gust profiles from 4 to 14 km over Cape Kennedy computed in the vehicle time domain (dots) and NASA MSFC design spectra (lines).

frequency, K(cycles/4000 m) can be transformed to PSD's in the time domain of vehicle flight, $\Phi(f)$ [(m/sec)²/(cycle/sec)] according to the simple relation, implied by Ryan et al.,[6]

$$\Phi(f) = 4 \times 10^3 \Phi(K)/v \quad (7)$$

where v is a vehicle vertical velocity arbitrarily chosen at the altitude of maximum dynamic pressure 12 km; for a Saturn vehicle v is 350 m/sec at 12 km and thus,

$$\Phi(f) = 11.4\Phi(K) \quad (8)$$

similarly f (cps) is a function of K,

$$f = Kv/4.10^3 = 0.0875K \quad (9)$$

As illustrated in Fig. 6, the PSD's at the 50% level for the MSFC design spectra are larger by a factor of 1.5 to 2 at all frequencies when compared to the PSD's computed from vehicle time domain profiles; similarly at the 95 and 99% levels for $f \leq 1.5$ cps, the MSFC design spectra are larger by factors of 1.4–1.7 and 2.2–2.7, respectively; for $f > 1.5$ cps the PSD's at the 95 and 99% level for the vehicle time domain, profiles decrease at a slower rate with increasing f and thus each is larger than the MSFC PSD's for $f > 2.5$ cps. These comparisons illustrate an apparent difference between spectra of profiles expressed in vehicle time coordinates and spectra of profiles in altitude coordinates; however, the transformation of the spectra from one coordinate system to the other implied by Eqs. (8) and (9) is strictly valid only when v is not a function of altitude; when v is a function of altitude, comparison of the spectra is not possible because a simple transformation does not exist. Therefore, the data given in Table 2 represent the best estimates, based on Jimsphere profiles, of the distribution of PSD at various frequencies as viewed by a Saturn vehicle; other estimates based on transformation of altitude domain spectra to the vehicle time domain using Eqs. (8) and (9) are not comparable.

Concluding Remarks

Following the approach suggested in an earlier study[1] of Jimsphere profiles, a set of gust profiles have been derived in the time domain of a Saturn vehicle. An analysis of these gust profiles has revealed that their spectrum densities are generally smaller than spectrum densities of altitude profiles conventionally transformed to the time domain by Eq. (7). It is suggested that the conventional transformation is invalid for time-dependent vehicle velocities and that the spectrum densities of the time-domain profiles derived in this study provide the most accurate estimate of the spectrum of horizontal wind speeds seen by a Saturn vehicle.

References

[1] Adelfang, S. I., Ashburn, E. V., and Court, A., "A Study of Jimsphere Wind Profiles as Related to Space Vehicle Design and Operations," CR-1204, Nov. 1968, NASA.

[2] Jacobs, D. B., "Saturn V AS-504 Launch Vehicle Reference Trajectory," Document DS-1548-1, Vol. 2, May 1967, The Boeing Co., Seattle, Wash.

[3] Alfriend, K. T., "Design of a Digital Filter for Application to Wind/Turbulence Data," LMSC/HREC 4710908, 1967, Lockheed Missiles & Space Co., Sunnyvale, Calif.

[4] Blackman, R. B. and Tukey, J. W., *The Measurement of Power Spectra*, Dover, New York, 1958.

[5] Fichtl, G. H., "In Flight Design Spectra of Atmospheric Turbulence," Marshall Space Flight Center Memo R-AERO-YE-182-69, Feb. 1969, NASA.

[6] Ryan, R. S., Scoggins, J. R., and King, A., "Use of Wind Shears in the Design of Aerospace Vehicles," *AIAA Journal*, Vol. 4, No. 11, Nov. 1967, pp. 1526–1532.

Momentum Imparted to Double-Sheet and Tubular Structures by Hypervelocity Impact

ROBERT H. MORRISON* AND C. ROBERT NYSMITH†
NASA Ames Research Center, Moffett Field, Calif.

THE meteoroid impact of a spacecraft, besides causing structural damage, can impart momentum to the spacecraft. If the momentum is large, this could cause appreciable rotation of the spacecraft and consequent loss of stabilization.

Although some data are available for the momentum imparted to very thick targets[1] and thin aluminum sheets[2] by hypervelocity impact, very little is known regarding the momentum imparted to structures more representative of spacecraft, such as double sheets or tubes. Available data[2,3] suggest that the imparted momentum depends on the state of the material sprayed from the rear of the impacted wall into the structure's interior. Calculations based on the method of Ref. 4 and employing the meteoroid environment of Ref. 5 indicate that a meteoroid impact at a velocity of 20 km/sec for some low-density metals, would cause the spray material to be melted partially. Conceivably, the liquid spray could undergo multiple reflections and attendant shock-heating within the walls of the structure, become vaporized and jet through the original entry hole to add appreciably to the imparted momentum. Moreover, in the case of a tube, the surface of the rear wall, by virtue of its curvature, could concentrate the reflected spray such that any jet effect, and, therefore, imparted momentum would be enhanced. On the other hand, the spray material could rupture the rear wall and escape, and not impart all of its momentum. To settle some of these questions, impact tests were conducted to determine the qualitative effects of various structural configurations on the momentum imparted to a spacecraft by a meteoroid impact.

The targets and projectiles were of aluminum, since calculations indicated that, by impacting this material at 7.8 km/sec, some of the spray would be melted. Thus, the state of the spray material for a meteoroid impact of a spacecraft would be simulated. A number of thin-walled targets of various configurations were impacted to determine the effects of some of the target variables. Each target was impacted near center in a direction approximately normal to the surface by a spherical projectile with a diameter of 3.18 mm. Since the projectiles were larger than meteoroids typically expected, the structural dimensions also were scaled up. Each target was mounted on a ballistic pendulum that measured the final target momentum. Also measured, by a separate pendulum, was the momentum of the material ejected uprange from the target. (See Ref. 2 for the techniques by which the momenta were measured.)

The configurations tested are shown in Fig. 1. Three tests were made with the first configuration, Fig. 1a, and are designated A, B, and C. The second configuration, Fig. 1b, differed from the first only in that it was a "closed" structure, with an aluminum tube inserted between the spaced sheets to prevent material from escaping except through the original entry hole or through the rupture, if any, in the rear wall. Two such targets, designated D and E, were tested. The third configuration (Fig. 1c) was an open-ended tube. Two tests, designated F and G, were made with this configuration. In all cases, the thickness of the front wall was 0.81 mm. This thickness was chosen to be one-fourth of the projectile diameter in order that a large percentage of the spray material would be melted (Ref. 6). The thickness of the rear wall was chosen, however, such that for each configuration one target would be ruptured but at least one other would not. The 1.6-mm-thick rear wall of target F was obtained by reinforcing the rear wall of a tube of constant wall thickness with a curved aluminum sheet.

In Table 1, the measured target momentum $(MV)_T$ and ejecta momentum $(MV)_E$, normalized with respect to the projectile momentum mv, are listed. (These ratios of momenta are used traditionally, for convenience, to report the results of momentum tests, but do not imply a sole dependence of either target momentum or ejecta momentum on projectile momentum.) In the last two columns of the table, the target and ejecta momenta are compared as ratios to the corresponding calculated momenta for a similar impact of a nonrupturing closed double-sheet target designated by $(MV)_{T\text{CALC}}$ and $(MV)_{E\text{CALC}}$. The calculations are based on the conservation of momentum and a correlation equation from Ref. 2

$$(MV)_{T\text{CALC}} = mv + (MV)_{E\text{CALC}} \quad (1)$$

$$(MV)_{E\text{CALC}} = mc(v - v_0)^2 \quad (2)$$

It is assumed in this calculation that there is no jet emerging from the hole. Here, m and v are the projectile mass and velocity, and the constants v_0 and c are equal to 0.55 km/sec and 0.017 sec/km, respectively. The former value is given by Ref. 2, whereas the latter was found by extrapolating the data of Ref. 2 to the lower front-sheet thickness of the targets impacted in the present tests.

A comparison of these ratios of momenta permits an assessment of the effects of jetting and rear-wall rupture on target momentum. Thus, if the jet emerging from the structure's interior is important, it would tend to enhance the target momentum so that $(MV)_T/(MV)_{T\text{CALC}} > 1$; whereas rear-wall rupture with no jet would reduce it, and $(MV)_T/(MV)_{T\text{CALC}} < 1$.

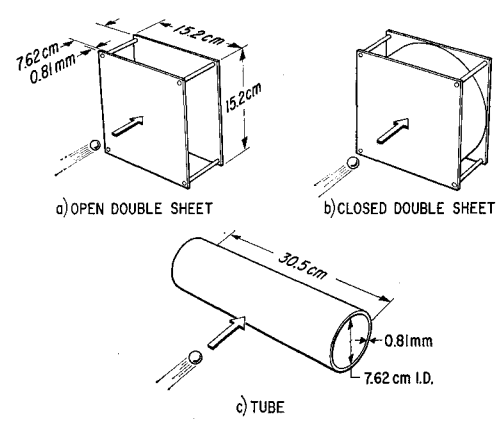

Fig. 1 Test configurations.

Received June 12, 1970.

* Research Scientist. Member AIAA.
† Research Scientist.